A00-36823

AIAA-00-3664

A Computational Study of Grid Erosion Through Ion Impact

I. D. Boyd
University of Michigan
Ann Arbor, MI 48109.

M. W. Crofton
The Aerospace Corporation
Los Angeles, CA 90009.

A COMPUTATIONAL STUDY OF GRID EROSION THROUGH ION IMPACT

Iain D. Boyd*

University of Michigan, Ann Arbor, MI 48109

Mark W. Crofton†

The Aerospace Corporation, Los Angeles, CA 90009

Abstract

A computer model is presented for predicting the erosion of electrostatic thruster grid sets due to energetic ion impact. The model employs a combination of a hybrid fluid-Particle In Cell method for the plasma dynamics, and the direct simulation Monte Carlo method for collision dynamics. The accuracy of the model is assessed through direct comparison with experimental measurements of grid currents for the UK-T5 ion thruster. The model accurately predicts the current collected on the acceleration grid for a range of operating points. The energy distribution of ions impacting on the grids is employed to compute the total mass of grid eroded during 10,000 hours of operation. The model significantly under predicts the current collected on the deceleration grid. However, analysis indicates that the missing decel current involves very low energy ion impact that would result in no significant increase in decel grid erosion.

Introduction

For ion engines, erosion of the accelerator and decelerator grids is a principal life-limiting process and a primary source of thruster-induced spacecraft contamination.[1-3] The usual grid material molybdenum is sputtered into the ion engine plume. It deposits on neighboring surfaces upon contact, leaving a metallic coating that alters surface properties and may affect the performance of solar arrays, sensors, and thermal control materials.

The limitation of lifetime due to erosion of the grids (primarily the accel grid but also the decel grid) exerts considerable influence on the choice of thruster type and rated thrust for the spacecraft. The end of life is usually taken at the point of grid mechanical failure due to extensive loss of the webbing. This results in loss of beam current capability and the onset of electron backstreaming into the discharge chamber. The erosion of grid material may also produce flakes which electrically short adjacent grids as may have temporarily occurred at the beginning of the Deep Space-1 mission. For the more than 60 ion engine endurance tests that have been reported, the majority of failure modes involved the accel grid.[1] To partially mitigate grid erosion effects, significant effort has been expended in the development of grids using erosion-resistant materials such as carbon-carbon composites[4] and titanium.[5]

* Associate Professor. Department of Aerospace Engineering.
† Research scientist. Space Materials Laboratory.

The purpose of the present study is to qualify a model that aims to predict ion thruster grid current collection and erosion. The model employs a combination of a fluid-Particle-In-Cell (PIC) approach[6] for electrostatics, and the direct simulation Monte Carlo (DSMC) method[7] for collisions. Collision mechanisms included in the code involve momentum transfer, charge exchange, and Coulomb interactions. The code solves the Poisson equation to determine the potential field.

In a previous study,[8] preliminary results were obtained using the model for the UK-T5 ion thruster. The UK-T5 employs a three-grid set in which the beam grid is set to 1060 V, the acceleration grid to -225 V, and the deceleration grid to -50 V. The present study will continue the investigation reported in Ref. 8 in two new directions. First, the current collected by the decel grid on the UK-T5 thruster will be considered. The second new aspect of the study will be to develop the capability to predict grid erosion rates. This will be achieved by computing the ion energy distribution function along each side of the grids directly from the simulation. The total mass of material eroded from the grids can subsequently be obtained by integrating sputtering yields for xenon ions impacting on the molybdenum grid material used in the UK-T5. A variety of operating conditions of the thruster are considered. These correspond to operating points tested experimentally at the Aerospace Corporation. The conditions for the experiments are listed in Table 1.

In the following, the experimental investigation is described briefly. More detailed information is provided in Ref. 8. Then, the computational model is discussed in detail. A variety of results is presented for a range of operating conditions of the thruster. These include general flow field properties, performance (thrust), accelerator grid current, ion energy distributions, and grid mass erosion.

Summary of Experimental Results

Details of the facility have been described previously.[2] The test chamber is 5.5 m in length and 2.4 m in diameter. Two custom reentrant cryopumps of combined 70,000 l/s pumping speed on xenon hang inside the chamber, suspended from flanges. During thruster operation at a nominal thrust level of 18 mN, the chamber pressure was determined to be 1.5×10^{-6} Torr, after applying a standard xenon-sensitivity correction to the indicated ion gauge reading. The thruster was mounted on a fixed stand in a side chamber with the ion beam directed across the main chamber. The beam dump consisted of aluminum plates covered with carbon-carbon composite panels, without water cooling. In the experimental study, two extraction grid sets of flight-quality (designated GS003 and GS004) were installed on the T5 ion thruster already characterized by past studies,[2] to perform design validation. In the present study, we will consider only the data obtained with the GS003 grid set. The current collected during the experiments on GS004 showed a decrease with time. While it is important for modeling efforts to be able to predict such behavior, this lies beyond the scope of the present investigation. The thruster is shown in Fig. 1. The anode was biased at the usual 1100 V operating point.[2] The screen grid and discharge chamber wall were about 40 V lower according to the value of the discharge voltage.

The screen and decel apertures were 2.15-2.18 mm in diameter, with a hole pitch of about 2.44 mm. The accel aperture diameter was 1.75-1.78 mm with similar pitch. Grids were 0.25 mm thick for screen and

decel grids, and 1.00 mm for the accel grid which was spaced 0.75 mm from the screen grid and 0.50 mm from the decel grid. Grid set GS003 had been previously operated for a period of roughly 50 hours at thrust levels around 18 mN. The mass flow rate was determined from calibrations of shunted flow rates with the engine off, monitoring the rate of pressure rise in a known volume. The absolute accuracy is better than 2% in each case. It was assumed that the flow rates measured with the engine off were identical to those obtained with the engine on.

The thruster characteristics at several operating points are listed in Table 1. The overall propellant mass utilization efficiency, η, includes both Xe^+ and Xe^{2+}. The fractional Xe^{2+} current, ζ, was estimated from measurements by Pollard.[9]

Modeling

Computer models of flow through ion grid apertures have been developed previously in several investigations. Among the first of these studies, Arakawa and Ishihara[10] employed a particle description of the ions. Neutral flow was neglected as was charge exchange. In the approach of Peng et al.[11], the ions were again treated using particles but in this case charge exchange was included by assuming a constant neutral flow field. More recently, similar studies have been reported.[12,13] In Refs. 10-13, only single charged ions were considered, and the treatment of the neutrals was simplified. In the present work, the ions and neutrals are treated in detail using a combination of two particle methods. A hybrid fluid-Particle-In-Cell approach (PIC)[6] is employed to model the plasma dynamics. In the present study, ions (both single and double charge states) are treated as particles. Following the work of Peng et al.[11] electrons are only assumed to exist in the regions upstream of the screen grid and downstream of the decel grid. This is a reasonable assumption based on the voltages applied to the grids. A fluid approach is employed for the electrons in which their temperature, T_e, is assumed to be constant, and their number density, n_e, is given by the Boltzmann relation:

$$n_e = n_{ref} \exp\left(\frac{\phi - \phi_0}{T_e}\right) \tag{1}$$

where ϕ is the local plasma potential and the electron temperature is in units of electron volts. In the region upstream of the screen grid, the reference potential, ϕ_0, is the discharge potential (1100 V), and the reference density, n_{ref}, is the plasma density of the discharge chamber. In the region downstream of the decel grid, the reference potential is 0 V and the reference density is taken to be 6×10^{15} m^{-3}. The Poisson equation is solved on a rectangular grid where the ion number density is given by the particles and the electron number density is given by Eq. (1). Following the approach of Roy et al.,[14] an Alternating Direction Implicit (ADI) method is employed to solve the Poisson equation which is non-linear due to the presence of ϕ in the above equation for the electron number density.

The second particle technique employed is the direct simulation Monte Carlo method (DSMC)[7] which is used to model collision phenomena. Thus, the neutral atoms are also treated as particles, and three different types of collisions are modeled: (1) charge exchange between Xe and Xe^+ and between Xe and Xe^{2+} using the cross sections measured recently by Pullins et al.[15]; (2) momentum transfer in which the cross sections are

given by the model of Dalgarno et al.;[16] and (3) Coulomb collisions. In charge transfer there is no momentum exchanged. In momentum transfer collisions, isotropic scattering in the center of mass frame is assumed. For Coulomb collisions, the equations from classical plasma physics for cross section and scattering angle are employed, e.g., see Ref. 17. However, the scattering angle for a particular collision is sampled statistically from the distribution suggested by Nanbu.[17] This procedure is necessary because DSMC-PIC is a statistical approach and the method does not compute intersecting particle trajectories deterministically. In Fig. 2, a selection of the collision cross sections employed in the present study is shown for the xenon system as a function of relative velocity. It is concluded that Coulomb collisions dominate at low collision energies. At high energies, the atom-atom momentum exchange and atom-ion charge exchange cross sections are of greatest significance. In Fig. 3, the variation of Coulomb scattering angle with relative velocity is shown. Here, it is evident that only very glancing interactions occur even at the low relative velocities which provide the largest cross sections (see Fig. 2).

The upstream boundary conditions for the DSMC-PIC approach involve specification of velocity distribution functions for each species. Under the assumption of thermal equilibrium in the discharge plasma, this is most conveniently achieved using Maxwell-Boltzmann distributions which requires specification of species number densities, velocities, and temperatures. The electron temperature is a very important parameter as it strongly influences electrostatic effects through the Boltzmann relation. It also determines the ion velocity upstream of the screen grid through the Bohm relation:

$$V_i = \sqrt{\frac{kT_e}{m_i}} \tag{2}$$

where k is Boltzmann's constant and m_i is the ion mass. A value of 5 eV is assumed for the electron temperature for most of the results presented in this study.

The flux of neutral atoms across a radial surface upstream of the screen grid is given by the standard result from kinetic theory:

$$\Gamma_a = \frac{1}{4} n_a V_a \tag{3}$$

where the mean molecular speed is given by:

$$V_a = \sqrt{\frac{8kT_a}{\pi m_a}} \tag{4}$$

In Eqs. (3)-(4), subscript a indicates properties of the atoms. The temperature of the neutral atoms is assumed to be 500 K. The atom and ion fluxes are computed so as to be consistent with the experimentally measured values of total beam current and mass flow rate. Thus, using Eqs. (2)-(4), the atom and ion number densities are determined. One further parameter that must be assigned is ζ, the fraction of ion current represented by Xe^{2+}. In Table 1, estimates are given for ζ based on the measurements of Pollard[9].

Finally, the ion temperature must be assigned to determine the distribution of ion velocities flowing into the computational domain. Most of the results presented in this study employ an ion temperature of 3.0 eV.

This value is consistent with experimental measurements made in an ECR argon plasma[18] using a plasma density and magnetic field that are similar to those employed in the plasma source of the UK-T5.

The computational grid employed in most of the simulations is shown in Fig. 4. The cell sizes are 20 to 40 μm, which are of the order of the Debye length for the conditions investigated. These sizes are orders of magnitude smaller than the mean free paths for all flow conditions. The time-step employed in all the simulations is 0.4 ns, and is a fraction of the reciprocal of the plasma frequency. The surfaces of the three grids are at fixed potentials and are assumed to have a constant temperature of 500 K. Ions striking any of the grids are assumed to recombine to neutral atoms. The facility back pressure is sufficiently low (0.2 mPa) such that it should have no effect on the flow through the grids. For completeness, it is included, and is assumed to consist of neutral xenon at a temperature of 300 K.

One of the main results from the computations is the ion current collected by the acceleration grid. This is computed by directly counting the number of ion particles impacting on any surface of the acceleration grid over a finite period of physical time. This procedure is also adopted for the current collected by the deceleration grid.

Results

General Flow Field Results

We first consider some general flow field properties for the case with a beam current of 399 mA. In Fig. 5, contours of plasma potential (in Volts) are shown. These show the sheath structure formed in front of the screen grid. The trajectories of the ions are shown in Fig. 6 and these illustrate how the grid configuration acts to accelerate most of the ions. It is expected that charge exchange ions will play a significant role in determining the grid currents. The volumetric production rate of charge exchange ions is given by:

$$\nu_{CEX} = n_i n_a < \sigma_{cex} g > \tag{4}$$

where n_i is the ion number density, n_a is the atom number density, σ_{CEX} is the Xe-Xe^+ charge exchange cross section, and g is the relative collision velocity. Contours of ν_{CEX} are shown in Fig. 7 and indicate that there are two regions where almost all of the charge exchange ions are created. The first production region is upstream of the screen grid. The production rate is high in this region because this is where the product of the ion and neutral number densities is highest. The charge exchange ions created in this first region are essentially the same as the beam ions since little electrostatic acceleration has taken place here. The second production region occurs in a thin layer just upstream of the acceleration grid. The production rate is high in this region due to a very large ion velocity. These charge exchange ions are significantly slower than the beams ions and can be readily accelerated onto either the accel or the decel grid.

To illustrate the macroscopic behavior of the computational model, Fig. 8 shows the variation of computed thrust as a function of beam current. The thrust levels shown in Table 1 are nominal values which assume that ζ and the beam divergence are both zero. They were obtained from the expression

$$F = I_{beam} \frac{m}{e} V_e \tag{1}$$

where V_e is the exhaust velocity and m/e is the mass to charge ratio. Using ζ from Table 1, individual Xe^+ and Xe^{2+} contributions to the thrust are determined. The sum is plotted in Fig. 8. In both these data and the simulations, the thrust has a nearly linear dependence on beam current. While there is some uncertainty in the specification of the discharge plasma properties, in particular the ion and electron temperatures and the fraction of Xe^{2+} current, over the entire operational range, the thrust predictions are in excellent agreement with the estimated data.

Grid Results

First, we consider the predictions of the total ion current collected on each of the grids. The results for the accel grid are shown in Fig. 9 as a function of the beam current. The predicted results provide excellent agreement with the measured data. The measurements exhibit variation with changes in both beam current and total mass flow rate. It is significant that the model is able to successfully capture these variations. It is also important to note that the model predictions are relatively insensitive to the values assumed in the discharge plasma for the electron temperature. Decreasing T_e from 5 eV to 3 eV increases the accel grid current by 10%. This is due to the fact that with the Boltzmann relation, the potential (and therefore the electric field) is proportional to the electron temperature. An increase in T_e means that the radial electric fields at the screen grid are stronger, thus pushing more of the ions radially inwards away from the accel grid. A decrease of 1 eV in the ion temperature decreases the accel grid current by about 20%. This is due to the reduced diffusion of ions in the direction perpendicular to the main beam flow. These results indicate that a significant fraction of the accel current is caused by direct impingement of beam ions. The sensitivity of the results to this parameter indicate the need for theoretical and experimental study of the ion temperature in the plasma sources of ion thrusters.

The results obtained for ion current collected on the decel grid are shown in Fig. 10. In all cases, the model under predicts the measured data by a significant amount. It is postulated that most of the decel grid current arises from charge exchange ions formed in the plume that flow upstream from the ion beam onto the grid. One possible source of additional decel current is from molybdenum ions sputtered from the accel grid.

The distribution functions of the impact energy of ions as they collide with the different faces of the accel and decel grids are computed from the simulations. The distribution for the barrel (lower) edge of the accel grid for the case where the beam current is 399 mA is shown in Fig. 11. The distribution indicates that the impingement current is made up of two different populations of ions. The majority of the ions are of high energy and these represent direct impacts of primary ions. However, there is also a second peak of the distribution at about 200 eV and these are clearly charge exchange ions. Since the sputter yield of xenon ions on molybdenum is a strong function of impact energy, the structure of the ion energy distributions will play a significant role in the determination of the overall grid erosion. In Fig. 12, the distribution function of impacting ions on the barrel of the accel grid is shown for the 218 mA beam current case. In this case, the relative populations of the low and high energy impacts is reversed from those shown in Fig. 11.

To obtain predictions of the total mass of grid eroded, the sputter yield for impact of xenon ions on molybdenum is integrated over the ion energy distributions such as those shown in Figs. 11 and 12. The sputter yield for an ion impacting on a solid surface is a function of impact energy and impact angle. An extensive review of sputtering processes for ion thrusters is provided by Duchemin et al..[19] In the present work, the experimental measurements of Weijsenfeld et al.[20] are used for the sputter yield of impacts normal to the surface. The measured data points are shown in Fig. 13 and show a near linear increase of yield with impact energy. The sputter yield for the incident energy of each impact recorded in the simulation is obtained from the measured data using linear interpolation or extrapolation. The angular dependence of sputter yield is estimated using the following empirical relation of Yamamura et al.[21]:

$$\frac{Y(\theta)}{Y(0)} = \cos^{-f}\theta \exp[-\Sigma(\cos^{-1}\theta - 1)]$$

where θ is the angle of incidence measured from the surface normal, and the constants f=19.96 and Σ=13.55 for 100 eV xenon ions impacting on molybdenum. This relation is shown in Fig. 14 where the maximum yield is indicated to occur at impact angles (relative to the normal direction) of about 47 deg..

The predictions of total grid mass eroded over 10,000 hours of operation for both the accel and decel grids are shown in Fig. 15. These results illustrate the importance of the energy dependence of the sputter yield. Comparison of Figs. 9 and 10 indicates that the model predicts a total current on the decel grid that is close to an order of magnitude lower than that collected on the accel grid. However, due to the larger average ion energy of the current on the decel grid, the total mass erosion for the decel grid is only a factor of about 3 lower than that for the accel grid.

It is appropriate to consider the effect on grid erosion due to the under prediction of decel grid current by the model. Let us assume that the remaining current arises from the back flow of ions from the plasma downstream of the decel grid. The maximum energy of these ions as they impact on the downstream face of the decel grid is about 50 V (i.e. the magnitude of the voltage applied to the decel grid). The sputter yield data shown in Fig. 13 indicate that this energy is near threshold. For the purpose of estimation, we take the average sputter yield at this impact energy to be 0.01. If it is assumed that 0.5 mA of decel grid current is contributed by the back flowing ions, then, over a 10,000 hour period, the total decel grid erosion due to the back flowing ions is approximately 0.2 g. Therefore, it is concluded that the predictions of decel grid erosion given in Fig. 15 essentially represent the total amount due to the fact that the missing decel current involves relatively low energy ion impacts.

Another possible source of additional decel current is from molybdenum ions sputtered from the grids. Any ions sputtered from the accel grid are likely to return to that grid due to its very low potential. Ions sputtered from the decel grid are most likely to return to that grid, but this current will obviously be very small. Finally, the molybdenum atoms sputtered from the accel grid may under go charge exchange interactions with the beam ions and some of these molybdenum ions may impact on the decel grid. The current associated with each of these scenarios is very small and indicates that these processes should not contribute significantly to the erosion processes.

Concluding Remarks

The level of agreement obtained between the predictions and experimental measurements for the current collected on the accel grid over a wide range of operating conditions is very satisfying. However, it is important to note that there are several important aspects of the model where improvements are required. The first of these concerns the significant under prediction of the decel currents. It was anticipated that most of the current on the decel grid would originate from the plasma downstream of the decel grid. Attempts to include this ion flux in the computations were unsuccessful. Any low energy ions introduced across the downstream boundary of the computational domain were at first accelerated towards the centerline of the aperture in the upstream direction. Eventually, these ions were again turned in the downstream direction, but they never impacted on the decel grid. This behavior indicates that a more detailed treatment of the plasma downstream of the thruster is required. However, as discussed above, the amount of sputtering caused by the missing decel current is negligible due to the low energy involved (on the order of 50 V). Processes involving sputtered molybdenum atoms and ions are unlikely to lead to significant erosion processes.

Another important limitation of the present model concerns the fact that the flow through a single aperture is used to predict the flow across the entire face of the grid. There is considerable variation in the observed erosion patterns across the face of a grid indicating that the plasma flow must also vary. Modeling of this variation requires development of a detailed model for the plasma discharge chamber. Related to this issue, is the fact that the discharge plasma properties are estimated in the present work. The computed grid currents exhibit relatively small variation (about 10%) for changes in the electron temperatures of 1–2 eV. It is significant that the model successfully predicts the accel grid current over a wide range of beam currents and flow rates. Finally, in computing the total mass erosion for 10,000 hours of operation, the present computations have neglected the change in geometry of the grids throughout the operation caused by the erosion. Erosion will of course increase the size of the apertures and this should lead to a decrease in grid currents and erosion mass. In addition, it should be noted that some fraction of the molybdenum sputtered from either grid may later become re-deposited on a grid. For each of these reasons, the data presented in Fig. 15 for grid erosion represent upper bounds.

Acknowledgments

The preparation of this manuscript was supported in part by The Aerospace Corporation through the Aerospace Independent Research and Development Program.

References

[1] Brophy, J.R., Polk, J.E., and Rawlin, V.K., "Ion Engine Service Life Validation by Analysis and Testing," AIAA Paper 96-2715, July 1996, and references therein.

[2] Crofton, M.W., "Evaluation of the United Kingdom Ion Thruster," *Journal of Spacecraft and Rockets*, Vol. 33, No. 5, 1996, pp. 739-747, and references therein.

[3] Fearn, D.G., "Ion Thrusters Lifetime Limitations Imposed by Sputtering Processes," IEPC Paper 93-177,

23rd International Electric Propulsion Conf., Seattle, Sept. 1993.

[4] Kitamura, S., Hayakawa, Y., Kasai, Y., and Osaki, T., "Fabrication of Carbon-Carbon Composite Ion Thruster Grdis-Improvement of Structural Strength," IEPC Paper 97-093, August 1997.

[5] Soulas, G. C., Haag, T. W., Patterson, M. J., and Rawlin, V. K., "Titanium Optics for Ion Thrusters," IEPC Paper 99-149, October 1999.

[6] Birdsall, C. K. and Langdon, A. B., *Plasma Physics Via Computer Simulation*, Adam Hilger Press, 1991.

[7] Bird, G. A., *Molecular Gas Dynamics and the Direct Simulation of Gas Flows*, Oxford University Press, 1994.

[8] Crofton, M.W., and Boyd, I.D., "The Origins of Accelerator Grid Current: Analysis of T5-Grid Test Results," AIAA Paper 99-2443, June 1999 (to appear in *Journal of Propulsion and power*).

[9] Pollard, J.E., "Plume Angular, Energy, and Mass Spectral Measurements with the T5 Ion Engine," AIAA Paper 95-2920, July 1995.

[10] Arakawa, Y. and Ishihara, K., "A Numerical Code for Cusped Ion Thrusters," IEPC Paper 91-118, October 1991.

[11] Peng, X., Keefer, D., and Ruyten, W., "Plasma Particle Simulation of Electro-static Ion Thrusters," *Journal of Propulsion and Power*, Vol. 8, No. 2, 1992, pp. 361-366.

[12] Nakano, M. and Arakawa, Y., "Ion Thruster Lifetime Estimation and Modeling Using Computer Simulation," IEPC Paper 99-145, October 1999.

[13] Tartz, M., Hartmann, E., Deltscew, R., and Neumann, H., "Validation of a Grid-Erosion Simulation By Short-Time Erosion Measurements," IEPC Paper 99-147, October 1999.

[14] Samanta Roy, R. I., Hastings, D. E., and Gatsonis, N. A., "Ion-Thruster Plume Modeling for Backflow Contamination," *Journal of Spacecraft and Rockets*, Vol. 33, No. 4, 1996, pp. 525-534.

[15] Pullins, S., Chiu, Y., Levandier, D, and Dressler, R., "Ion Dynamics in Hall Effect and Ion Thrusters: $Xe^+ + Xe$ Symmetric Charge Transfer," AIAA Paper 00-0603, January 2000.

[16] Dalgarno, A., McDowell, M. R. C., and Williams, A., "The Mobilities of Ions in Unlike Gases," *Proceedings of the Royal Society*, Vol. 250, 1958, pp. 411-425.

[17] Nanbu, K., "Theory of Cumulative Small-Angle Collisions in Plasmas," *Physical Review E*, Vol. 55, No. 4, 1997, pp. 4642-4652.

[18] Sadeghi, N., Nakano, T., Trevor, D. J., and Gottscho, R. A., "Ion Transport in an Electron Cyclotron Resonance Plasma," *Journal of Applied Physics*, Vol. 70, 1991, pp. 2552–2569.

[19] Duchemin, O. B., Brophy, J. R., Garner, C. E., Ray, P. K., Shutthandan, V., and Manteniekssm M. A., "A Review of Low Energy Sputtering Theory and Experiments," IEPC Paper-97-068, September 1997.

[20] Weijsenfeld, C. H., Hoogendoorn, A., and Koedam, M., "Sputtering of Polycrystalline Metals by Inert Gas Ions of Low Energy (100-1000eV)," *Physica*, Vol. 27, 1961, p. 763.

[21] Yamamura, Y., Itikawa, Y. and Itoh, N., "Angular Dependence of Sputtering Yields of Monatomic Solids," Report IPPJ-AM-26, Institute of Plasma Physics, Nagoya University, Japan, 1983.

Table 1. Operating data for grid set GS003.

I_{beam}	$\dot{m}$	η	ζ	V_{beam}	V_{acc}	V_{dec}	I_{acc}	I_{dec}	F
(mA)	(mg/s)	(-)	(-)	(V)	(V)	(V)	(mA)	(mA)	(mN)
218	0.359	0.754	0.170	1100	-225	-50	0.53	0.25	11.9
270	0.482	0.720	0.105	1100	-225	-50	0.90	0.44	14.8
327	0.626	0.685	0.070	1100	-225	-50	1.43	0.69	17.9
328	0.551	0.759	0.126	1100	-225	-50	1.10	0.46	17.9
348	0.551	0.790	0.161	1100	-225	-50	1.05	0.38	19.0
363	0.626	0.751	0.094	1100	-225	-50	1.37	0.55	19.9
399	0.626	0.798	0.159	1100	-225	-50	1.25	0.40	21.8

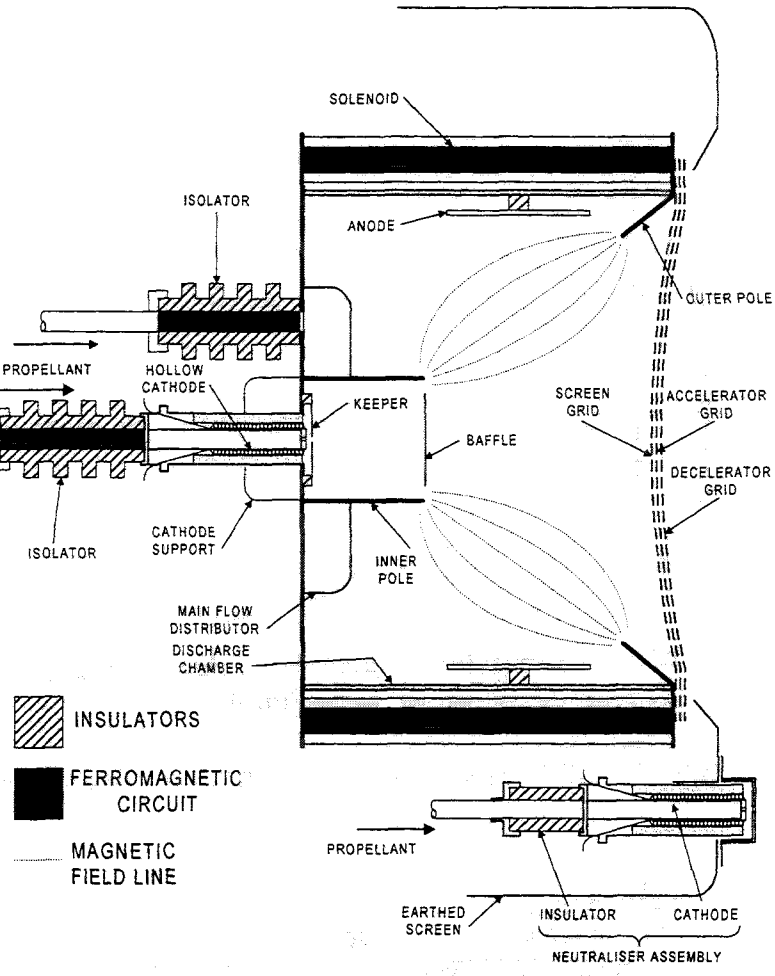

Fig. 1. Schematic diagram of the UK-T5 thruster.

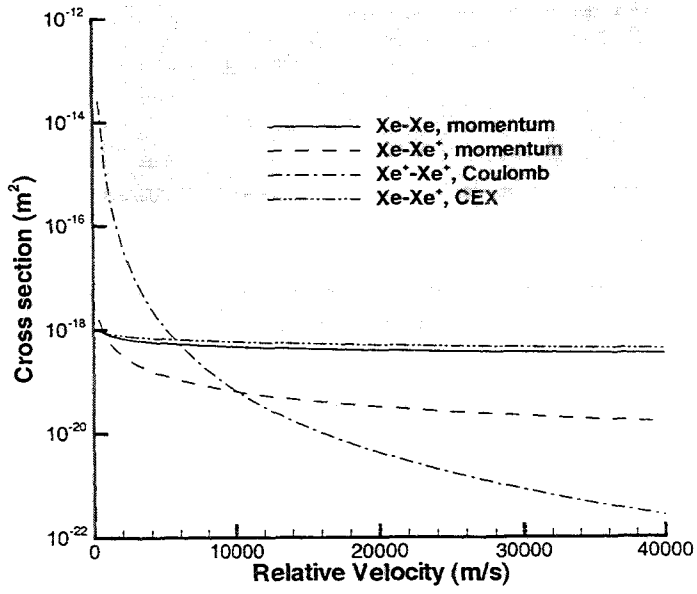

Fig. 2. Various collision cross sections as a function of relative velocity.

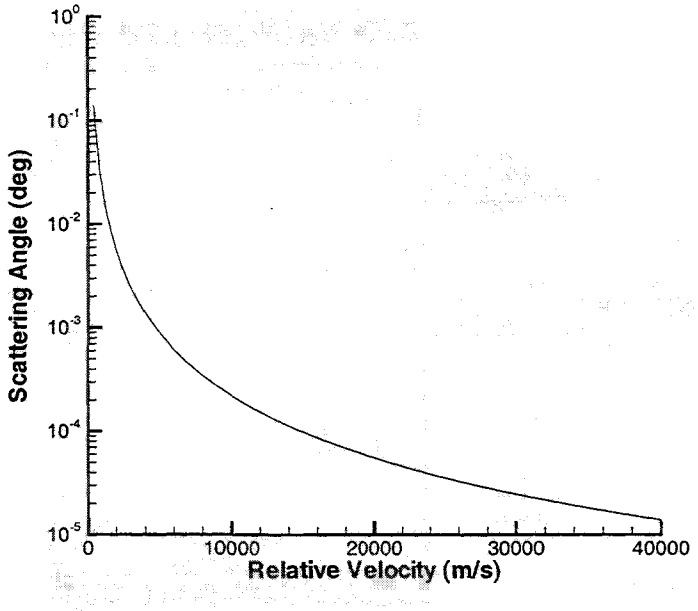

Fig. 3. Coulomb collision cross section as a function of relative velocity.

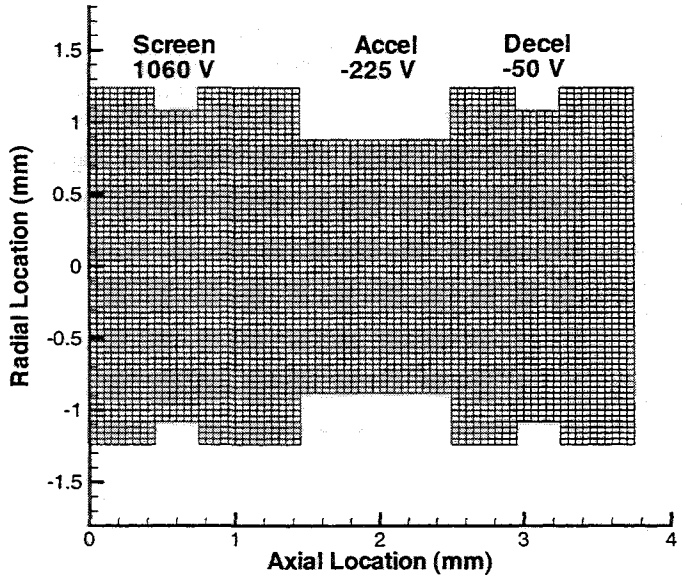

Fig. 4. Computational grid.

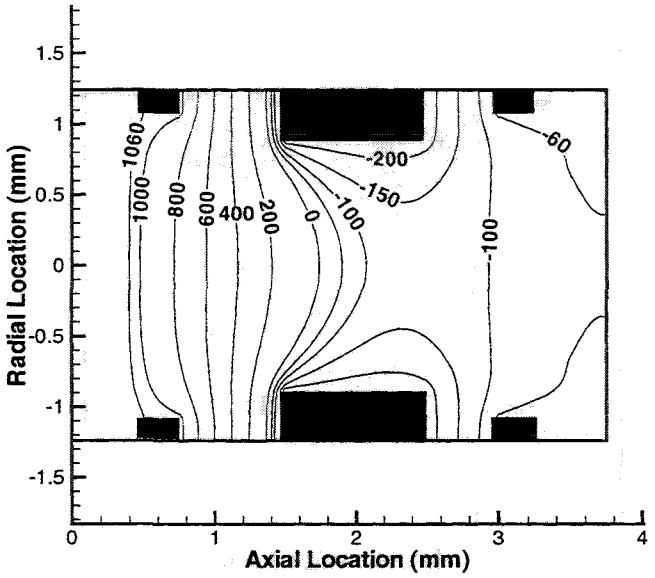

Fig. 5. Contours of plasma potential.

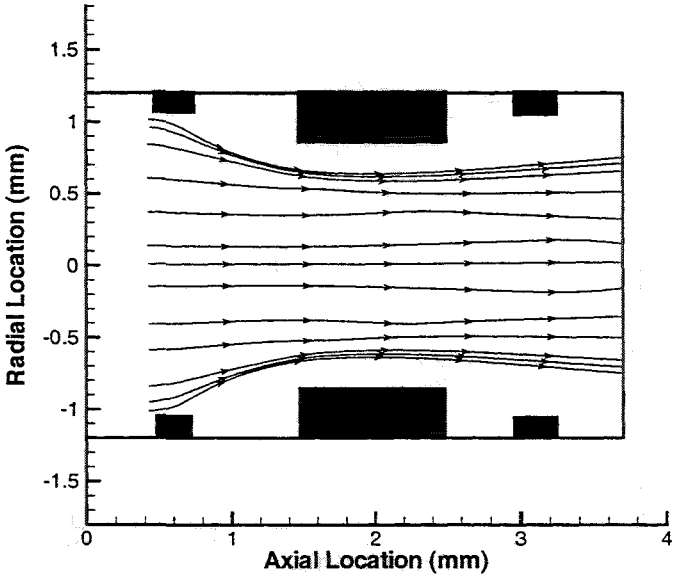

Fig. 6. Streamlines of the ions.

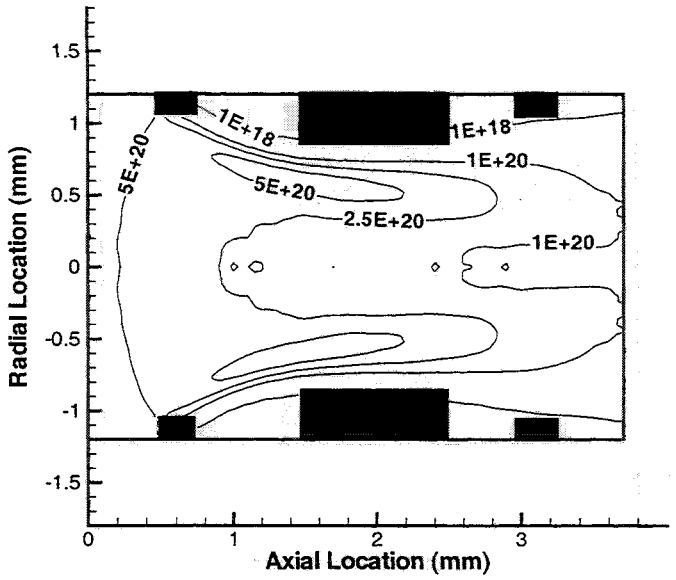

Fig. 7. Contours of volumetric production rate of charge exchange ions (m^{-3} s^{-1}.

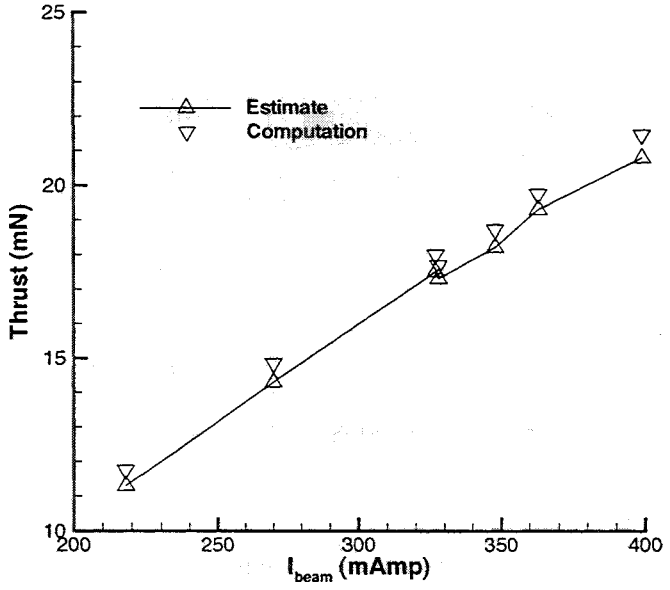

Fig. 8. Thrust as a function of beam current.

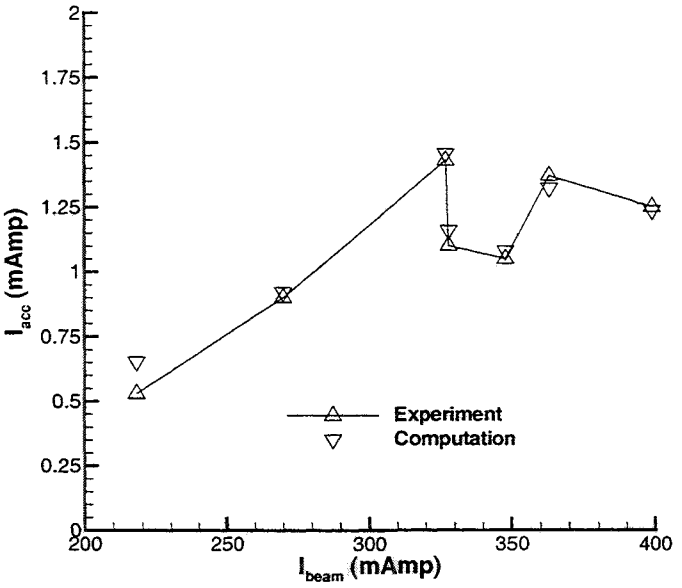

Fig. 9. Current collected on the acceleration grid as a function of beam current.

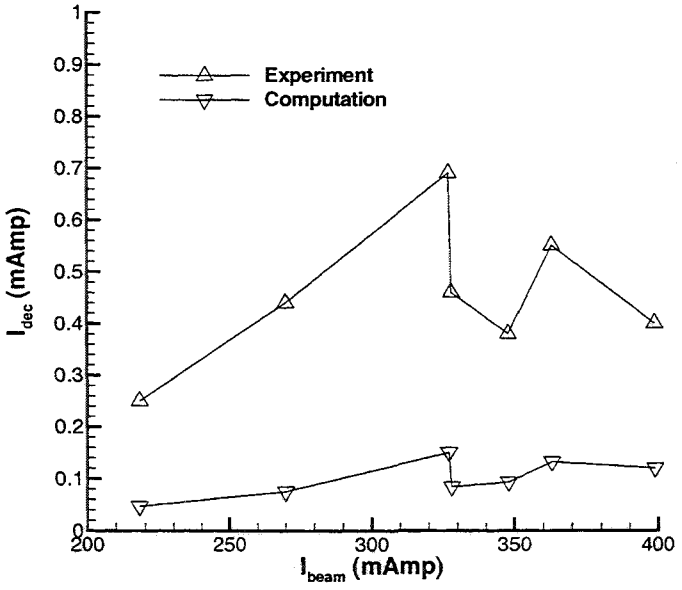

Fig. 10. Current collected on the deceleration grid as a function of beam current.

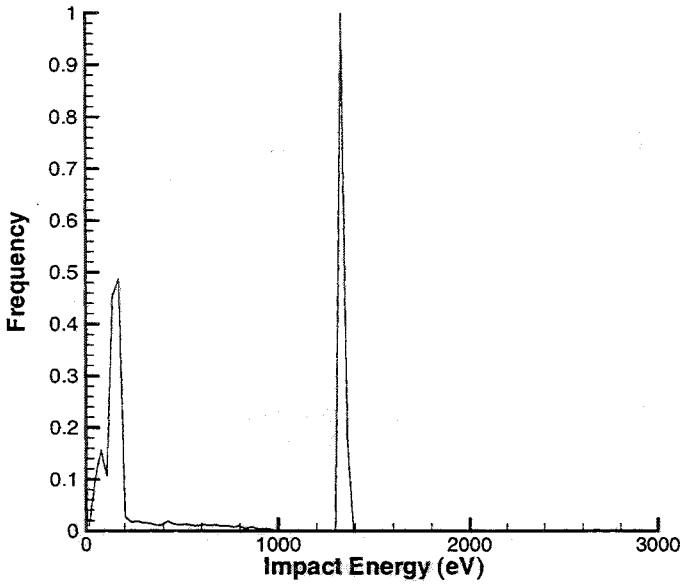

Fig. 11. Ion energy distribution function on the barrel of the acceleration grid at 399 mA beam current.

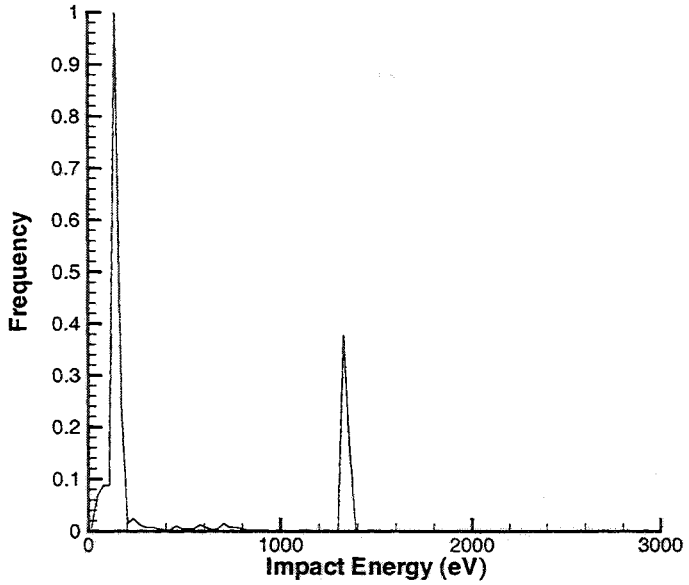

Fig. 12. Ion energy distribution function on the barrel of the acceleration grid at 218 mA beam current.

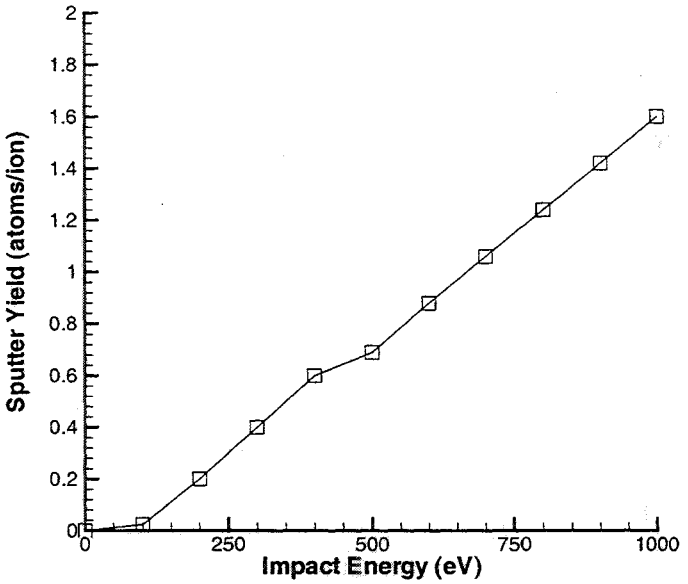

Fig. 13. Sputter yield measurements of xenon ions impacting on molybdenum from Ref. 20.

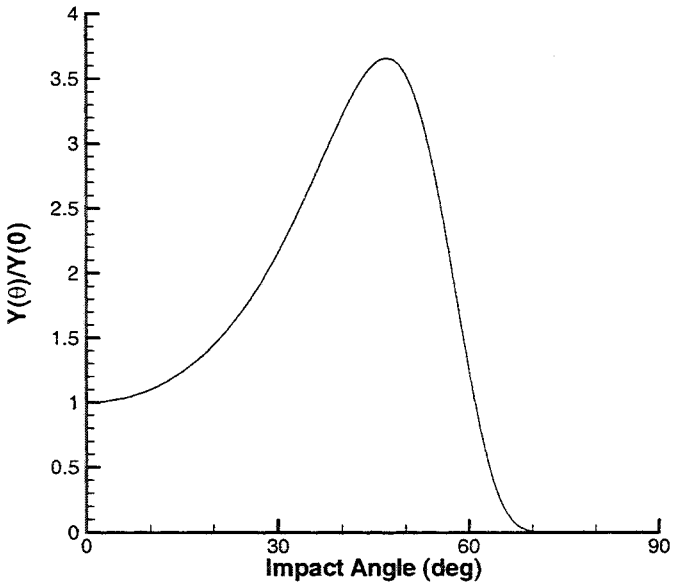

Fig. 14. Angular dependence of sputter yield for xenon ions impacting on molybdenum from Ref. 21.

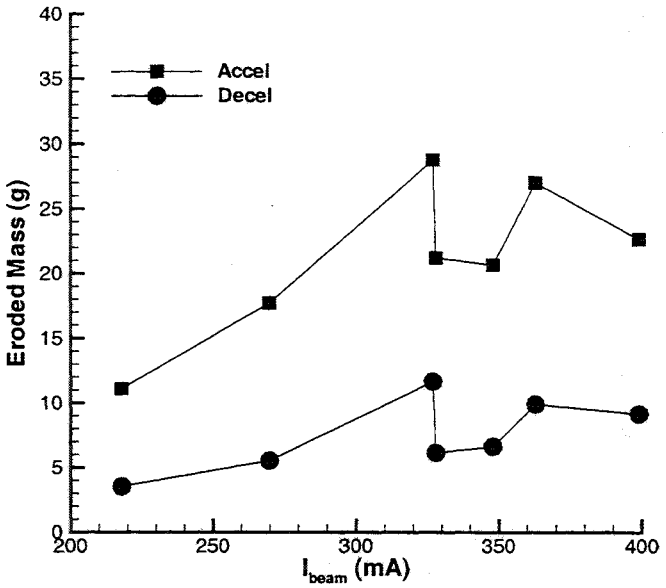

Fig. 15. Predictions for total mass erosion of the accel and decel grids for 10,000 hours of operation.